



HAL
open science

scCVD diamond membrane based microdosimeter for hadron therapy

Izabella Zahradnik, Michal Pomorski, Ludovic de Marzi, Dominique Tromson,
Philippe Barberet, Natko Skukan, Philippe Bergonzo, Guillaume Devès, Joël
Herault, Wataru Kada, et al.

► To cite this version:

Izabella Zahradnik, Michal Pomorski, Ludovic de Marzi, Dominique Tromson, Philippe Barberet, et al.. scCVD diamond membrane based microdosimeter for hadron therapy. *Physica Status Solidi A (applications and materials science)*, 2018, 215 (22), pp.1800383. 10.1002/pssa.201800383. cea-04146874

HAL Id: cea-04146874

<https://cea.hal.science/cea-04146874v1>

Submitted on 30 Jun 2023

HAL is a multi-disciplinary open access archive for the deposit and dissemination of scientific research documents, whether they are published or not. The documents may come from teaching and research institutions in France or abroad, or from public or private research centers.

L'archive ouverte pluridisciplinaire **HAL**, est destinée au dépôt et à la diffusion de documents scientifiques de niveau recherche, publiés ou non, émanant des établissements d'enseignement et de recherche français ou étrangers, des laboratoires publics ou privés.

scCVD Diamond Membrane based Microdosimeter for Hadron Therapy

Izabella A. Zahradnik,^{1,*} Michal T. Pomorski,^{1,*} Ludovic De Marzi², Dominique Tromson³, Philippe Barberet^{4,5}, Natko Skukan⁶, Philippe Bergonzo⁷, Guillaume Devès^{4,5}, Joël Herault⁸, Wataru Kada⁹, Thierry Pourcher^{10,11}, Samuel Saada¹

- 1 I. A. Zahradnik, Dr. M. T. Pomorski, Dr. S. Saada. CEA-LIST, Diamond Sensors Laboratory, 91191 Gif-sur-Yvette, France. E-mail: izabella.zahradnik@cea.fr; michal.pomorski@cea.fr
- 2 Dr. L. De Marzi. Institut Curie, Centre de Protonthérapie d'Orsay, 91400 Orsay, France
- 3 Dr. D. Tromson. CEA-LIST, Sensors and Electronic Architectures Laboratory, 91191 Gif-sur-Yvette, France
- 4 Dr. P. Barberet, Dr. G. Devès. Université de Bordeaux, CENBG, Chemin du Solarium, 33175 Gradignan, France
- 5 Dr. P. Barberet, Dr. G. Devès. CNRS, UMR5797, CENBG, Chemin du Solarium, 33175 Gradignan, France
- 6 Dr. N. Skukan. Division of Experimental Physics, Ruder Boskovic Institute, 10000 Zagreb, Croatia
- 7 Dr. P. Bergonzo. CEA-LIST, 91191 Gif-sur-Yvette, France
- 8 Dr. J. Herault, Centre Antoine-LACASSAGNE, Institut Méditerranéen de Protonthérapie, 06189 Nice, France
- 9 Dr. W. Kada, Faculty of Science and Technology, Gunma University, Kiryu, Gunma 376-8515, Japan
- 10 Dr. T. Pourcher. CEA, Laboratoire TIRO, 06189 Nice, France
- 11 Dr. T. Pourcher. Université de Nice-Sophia Antipolis, University Côte d'Azur, 06189 Nice, France

Abstract

Hadron therapy is an innovative mode of radiotherapy (RT) for cancer treatment which enables tumor cells to be more effectively destroyed than conventional RT using photons. The precise knowledge of the lineal energy of particles is used in the field of microdosimetry (MKM model) as a fundamental parameter in the prediction of the relative biological efficiency (RBE) of clinical beams. Based on single-crystal CVD (scCVD) super-thin diamond membranes obtained using deep Ar/O₂ plasma etching, prototypes of solid-state microdosimeters for lineal energy measurements are produced at the Diamond Sensors Laboratory of CEA-LIST. The response of a diamond membrane microdosimeter to single projectiles is investigated in ion microbeams. The microdosimeter is irradiated using a raster scanning method and the charge transport properties of the device are determined with sub-micron precision by measuring the charge collection efficiency (CCE), the μ SVs 3D spatial definition and the pulse-height spectra. A prototype of this novel microdosimeter is then tested in a 100 MeV therapeutic proton beam at the Institut Curie – Proton Therapy Centre in Orsay. All results effectively demonstrate the great potential for this device to be used for studies of the RBE in clinical applications.

Keywords

diamond microdosimeter, hadron therapy, ion beam induced charge, lineal energy, microdosimetry, micro-sensitive volumes

1 Introduction

In the 21st century, death due to cancer is still a major issue on a global scale. According to the 2017 annual report of the World Health Organization an estimated 8.8 million deaths occurred due to cancer worldwide in 2015, accounting for 22% of all deaths [1]. The most common treatment methods of cancer are invasive surgery, chemotherapy, radiotherapy, or combinations of these. Each year approximately 30% of cancer patients worldwide are treated using external radiotherapy (RT). Most of the external RT treatments are based on irradiating tumors with photons. However, hadron therapy

(using protons or carbon ions) is an innovative and very promising mode of RT for cancer treatment. It enables tumor cells to be more effectively destroyed than conventional radiation therapy using photons [2].

Charged particles exhibit the advantage of having an inverse depth dose distribution in comparison to photons. This kind of distribution implies the increase of the dose with penetration depth up to a maximum at the end of the particles path with the highest energy loss (Bragg peak). This advantage maximises the dose to the cancer region and spares as much as possible of the healthy tissue. By using hadron therapy, the dose to the surrounding of the tumor's tissue can be reduced by around 60% compared with modern intensity-modulated radiation therapy (IMRT) with photons [3]. Alongside the physical advantages, ion beams additionally show an increased relative biological effectiveness (RBE), which is defined as the ratio of the irradiated dose of ions to that of a reference photon energy that would be required to result in the same biological effect for both [2]. This increased effectiveness can be explained by the different microscopic energy deposition patterns of photons and ions. Finally, these mentioned properties make the therapy with ions highly attractive for challenging radioresistant tumors.

Due to the advantages of hadron therapy and thus its increasing interest, a treatment planning system based on radiobiological effects needs to be considered. This system is supposed to ensure a safe dose delivery to the treated patients and is important to fully exploit the advantages of all relevant ions for this kind of therapy. The RBE of ions in tissue is one of the most significant parameters to be considered for the radiobiological treatment planning. Worldwide, there are two clinically employed radiobiological models for the prediction of the RBE in hadron therapy: the local effect model (LEM), which is a pure theoretical model and based on track structure [4] and the microdosimetric kinetic model (MKM) [5] based on measured microdosimetric quantities.

In routine clinical proton therapy, a constant RBE value of 1.1 is being used as the golden standard [6] despite a high number of publications on this subject, as is summarized in Paganetti [6], clearly showing that the RBE changes even for light ions with different linear energy transfer (LET) values in clinical beams. As a result, a radiobiological optimization of the treatment plans based on simulated dose averaged LET values has been introduced in Paganetti [6] and Grassberger et al. [7].

In radiotherapy, the value of the LET is used to describe the average energy deposited per unit length (in $\text{keV } \mu\text{m}^{-1}$) in an absorber material e.g., biological cell or tissue. However, serious limitations of the LET concept with respect to the RBE and radiation quality have been discussed in the ICRU report no.16 [8]. These limitations in LET values resulted in developing a set of measurable stochastic quantities in volumes compared in size to a human cell, such as lineal energy of particles, which would provide the fundamental basis for microdosimetry [9]. The lineal energy is used to describe the energy deposited by a single event, namely ϵ , in a micron-size sensitive volume (SV), along the mean particle track length, \bar{l} , which according to [8] is given by:

$$\gamma = \frac{\epsilon}{\bar{l}} \quad (1)$$

Furthermore, due to the random fluctuations of the measured lineal energy, its probability distribution is also an important function for microdosimetric studies. From the measured data it is possible to display the dose lineal energy distribution, $d(\gamma)$. More details on microdosimetric quantities can be found in ref. [8].

A first device capable of measuring spectra of pulse-heights from each individual event in a microscopic scale was a low pressure proportional counter called "Rossi," which was developed in the early 1950s [10]. Today, several devices such as the tissue equivalent proportional counter (TEPC) or silicon-based semiconductor microdosimeter are commercially available or still being developed. Both types of these micro-detectors are well studied and documented in the following literature [9, 11]. In the pioneering and commercial TEPC technique, a tissue-equivalent gas (propane-based) is used for measuring microdosimetric quantities. However, limitations of the TEPC method with respect to microdosimetry include the high-voltage and the gas system, both of which are needed for operating the device. Pulse pile-up problems, as well as the low spatial resolution of the TEPC due to its relatively large size (cm), are also further limitations.

Solid-state detectors, such as silicon-based microdosimeters, have been developed over the last 20 years at the Centre for Medical Radiation Physics (CMRP) of the University of Wollongong in Australia. The last generation of silicon-based devices is called the “bridge” [12] and “mushroom” [13] microdosimeters. Their use in lineal energy measurements offers high spatial resolution and counting rates at low costs [9]. Using the new generation of silicon-based microdosimeters, a good agreement with the results from the well-established TEPC was possible. Furthermore, better spatial resolution and rate capability was observed for silicon-based detectors [9].

Although, a frequently raised issue is the question of tissue equivalence in the case of silicon material ($Z=14$), leading to complex correction factors when compared to e.g., diamond material ($Z=6$). Further advantages such as the radiation hardness and physical properties e.g., a large-band gap, temperature stability, fast drift velocity and low capacitance, make diamond an interesting potential material for producing microdosimetric devices. At present, significant developments in diamond-based microdosimeters with different approaches have been made at the Tor Vergata University [14] in Italy and at the CMRP [15]. Although so far, none of them has fully succeeded to obtain a functional device appropriate for microdosimetric quantity measurements in clinical beams.

For more than 10 years, CEA-LIST has been developing diamond dosimeters for RT applications. The starting point of the research was the development of dosimeters for complex photon irradiation beams such as IMRT or stereotactic beams and continued with dosimeters designed for high dose-rate proton beams [16, 17]. Currently, based on scCVD diamond membranes, new prototypes of microdosimeters are being developed at the CEA-LIST-Diamond Sensors Laboratory (LCD). The primary aim of this paper is to introduce these innovative microdosimeter prototypes to the scientific community.

2 Material and Methods

2.1 Diamond Microdosimeter Concept

Figure 1 shows the schematic diagram of a single micro-sensitive volume (μSV) of a scCVD diamond membrane based microdosimeter prototype. The top layer (in green) of the μSV consists of a thin (approx. 400 nm) layer of homoepitaxial boron-doped diamond (p^+). This layer is deposited onto an intrinsic diamond membrane (i) with a typical thickness of 1–3 μm (in blue). This layer can be shaped into the desired forms and sizes. Typically, μSV s with a side length of between 25 and 100 μm are produced, which is comparable in size to a human cell. On the bottom side of the membrane an electrical contact kept at the ground potential (in gray) is assured by a large pad electrode.

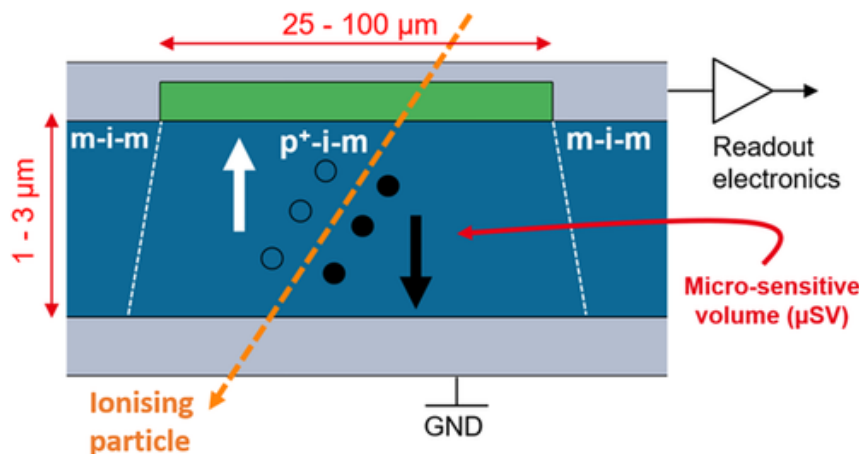


Figure 1 Simplified schematic diagram illustrating the configuration design of one self-biased micro-sensitive volume of the scCVD diamond membrane based microdosimeter. The device contains three different layers including the boron doped diamond (p^+) (in green), an electronic grade diamond (i) (in blue) and the electrical contacts based on metal or carbon (m) (in gray). During irradiation with ions (orange dashed arrow) charge drift at 0 V is possible due to the built-in potential within p^+ -i-m junction of the μSV .

This pad can be made of metal- or carbon-based material (m). Additionally, the top p⁺-diamond layer is interconnected with other μSVs, also by the same electrical contact (m) deposited on top of the structure, which is finally fed into the readout electronics (in grey).

Two different junction regions can then be distinguished within such a microdosimeter configuration, namely the p⁺-i-m junction inside of the μSV, and the m-i-m junction outside of it. The charge transport within the μSV and outside of it is schematically illustrated as a band-diagram in Figure 2. Due to the p⁺-i-m junction, as shown in Figure 2a, the bands bend resulting in an experimentally measured built-in potential of 1.8 V [18]. When an ionization event inside of the μSV occurs, excess charge carriers – electrons and holes – are generated and start to drift in the presence of a built-in electric field. These then induce the current signal in the readout electronics. No device biasing is needed in this configuration. By integrating the induced current signal (I), it is possible to obtain the collected charge (Q) with a 100% charge collection efficiency (CCE). This CCE is then directly proportional to the energy deposited by a single ionization event.

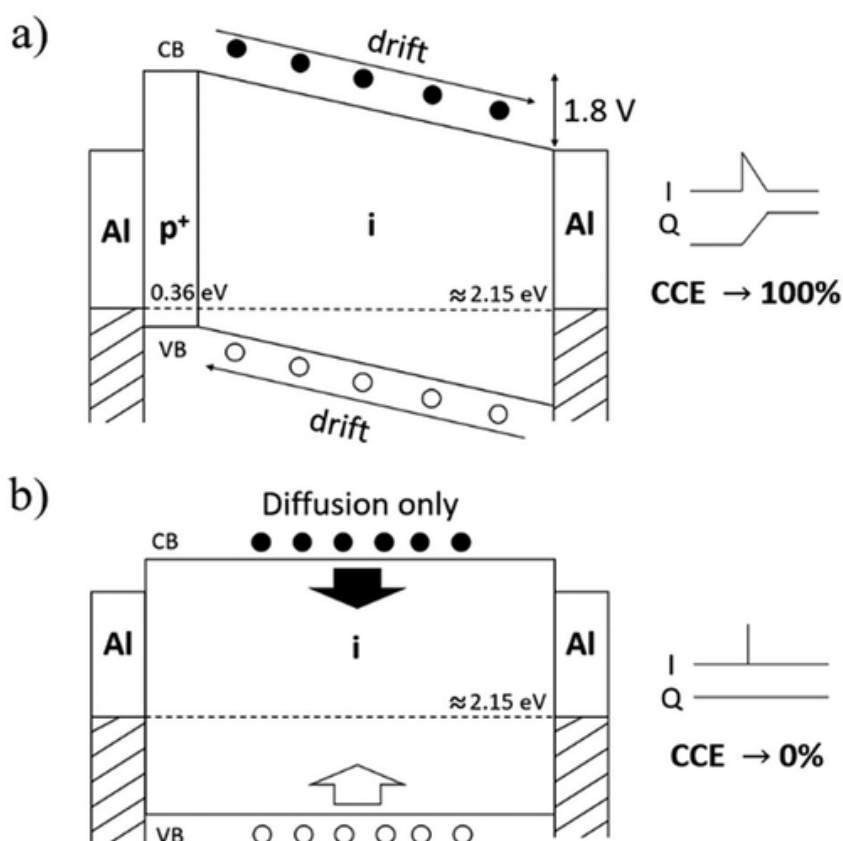


Figure 2 Band structures representing the signal formation a) within and b) outside one single μSV of a scCVD diamond membrane based microdosimeter. When the microdosimeter is irradiated with ionizing radiation, due to natural potential difference of the p⁺ and the intrinsic diamond (i) layer, charge drift at 0 V (applied external bias) inducing the current signal is possible. By integrating the induced current signal (I), it is possible to obtain the collected charge (Q) with a 100% charge collection efficiency (CCE). In the area outside of the μSV, only isotropic diffusion takes place and no current signal is generated.

The region outside of the μSV is illustrated in Figure 2b. Here no p⁺-i-m junction formation takes place, thus a built-in potential or a residual electric field can only be generated if non-perfect ohmic contacts are formed. The created excess charges carriers can only undergo isotropic diffusion, with no directional drift.

However, it is worth noting that for this particular diamond membrane microdosimeter setup, certain possible signal distortions need to be considered. For example, if ionization appears outside yet still

within the direct vicinity of the μSV , a part of the charge cloud diffuses into the μSV region and undergoes drift diffusion or partial extension of the electric field from p^+ -layer. This could cause signal formation with a reduced CCE, however this must be verified with detailed electric field simulations in the near future. Similar effects of reduced CCE from the edge of the active volumes have been also observed in Cazzaniga et al. [19] for other metal-diamond-metal structures however when applying bias voltage. It is also possible to have surface-pinning states or m-i-m regions if perfect ohmic contact is not achieved between the metal and diamond. This could also result in partial drift and thus residual signal formation with a reduced CCE.

2.2 Diamond Membrane Microdosimeter Prototyping

The scCVD diamond membrane based microdosimeter investigated in this study is based on an electronic grade scCVD diamond from Element Six, UK [20] and was produced at the CEA-LIST Diamond Sensors Laboratory (LCD) in France.

In Figure 3, the six steps of the membrane production are presented. Firstly, Figure 3a,b) electronic grade single crystal diamonds with a thickness of ca. 300–500 μm are sliced and polished by Almax easyLab in Belgium [21]. The cut slices result in a thickness of only 20–60 μm with surfaces parallelism below 1 μm on all sample surface. Afterwards, Figure 3c) a thin boron-doped diamond layer (p^+) on the top of a polished intrinsic diamond (i) is grown [22] For this purpose, a thin highly boron-doped single crystal diamond layer is produced via chemical vapor deposition (CVD) onto the surface of the intrinsic diamond slab. To create a below 10 μm thick membrane suspended over bulky frame, a deep Ar/ O_2 plasma etching is used Figure 3d) [23].

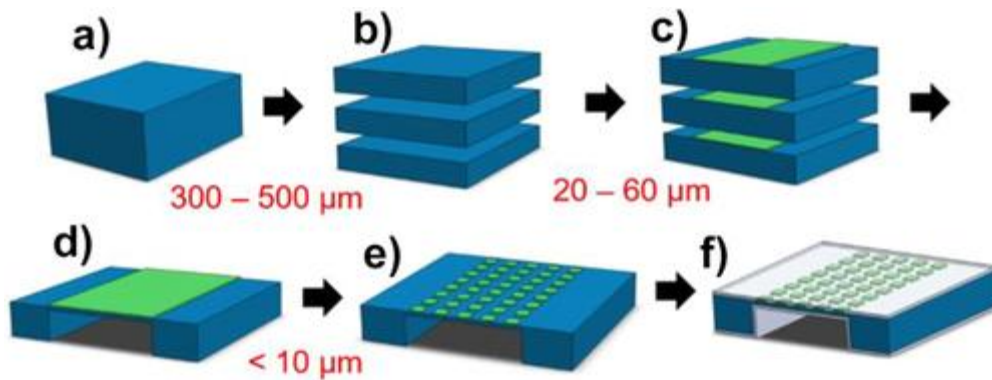


Figure 3 Production steps of the scCVD diamond membrane based microdosimeter. a,b) Slicing and polishing of the intrinsic diamond. c) CVD growth of a thin boron-doped diamond layer (p^+). d) Creation of a thin $<10\ \mu\text{m}$ diamond membrane due to deep Ar/ O_2 plasma etching technique. e) Patterning and shallow Ar/ O_2 etching of p^+ layer for the realization of multiple μSVs . f) PVD deposition of electrical contacts (metal- or carbon-based) on the top and bottom of the diamond membrane based microdosimeter.

This step is followed by Figure 3e) a photolithographic patterning of the p^+ layer with a deposited metal mask and a successive shallow Ar/ O_2 plasma etching step. Various shaped pixels defining the microdosimeter's μSVs can be produced in this manner. Finally, Figure 3f) the metal- or carbon-based electrical contact can be deposited on the back side of the membrane in a form of a full pad electrode. Similarly, on top of the membrane a second electrical contact must be deposited, interconnecting the μSVs with tracks, strip or pad electrodes.

In Figures 4 and 5, a 3D and scanning electron microscope (SEM) images of the scCVD diamond membrane based microdosimeter as used in this study are presented. For this microdosimeter prototype, both electrical contacts are made from Aluminum, deposited by physical vapor deposition (PVD) and using shadow masks. The various size ($25 \times 25\ \mu\text{m}^2$, $45 \times 45\ \mu\text{m}^2$, and $90 \times 90\ \mu\text{m}^2$) μSVs are connected by a 500 μm wide and 3 mm long single strip upper electrode.

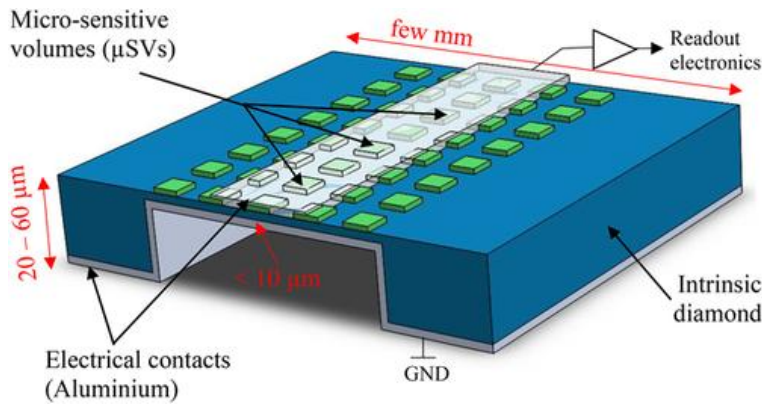


Figure 4 3D image of the scCVD diamond membrane based microdosimeter as used in this study. The electrical contacts are based on Aluminium. Only one single strip upper electrode is used for studying charge collection.

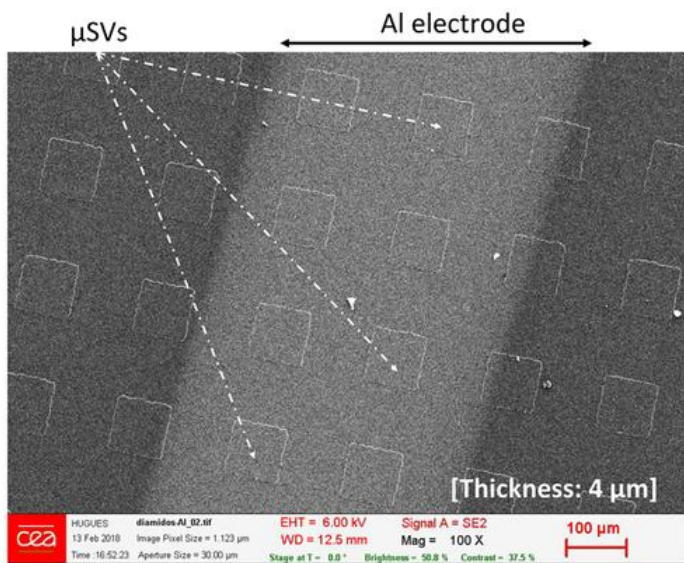


Figure 5 Scanning electron microscope (SEM) image of a sample Al strip region of the scCVD diamond membrane based microdosimeter prototype with micro-sensitive volumes (μ SVs), as used in this study. The square-shaped sensitive volumes were created in three different sizes: $25 \times 25 \mu\text{m}^2$, $45 \times 45 \mu\text{m}^2$, and $90 \times 90 \mu\text{m}^2$ (not all shown in this image).

These presented μ SVs are in their size comparable with the silicon state-of-the-art microdosimeters [9] and much smaller than related state-of-the-art diamond-based devices i.e., one macro SV ($200 \times 200 \mu\text{m}^2$) from Tor Vergata University [14]. The resulting thickness of the scCVD diamond membrane for detecting ionization events is $4 \mu\text{m}$. This thickness is again much smaller than the related state-of-the-art diamond-based devices with i.e., $30\text{--}500 \mu\text{m}$ thick CVD diamond samples used at CMRP [15].

2.3 Charge Transport Studies with the Ion Beam Induced Charge Technique

The charge collection efficiency for the scCVD diamond membrane based microdosimeter was investigated using the ion beam induced charge technique (IBIC). Essentially, a focused ion beam is raster scanned across the microdosimeter membrane. The single ion induced current (I) signals are then individually amplified and integrated resulting in a measured collected charge (Q), which is then digitalized and stored together with the coordinates for the position of the microbeam. The spatial position, along with the area and the CCE of the micro-sensitive volumes, can be determined accurately using this method. A more detailed description can be found in [24-26].

For this study, 16.6 carbon and 2.0 MeV proton microbeams were used. The access to the carbon ions nuclear microprobe was provided by the Laboratory for Ion Beam Interactions, Ruđer Bošković

Institute in Zagreb, Croatia [24]. This facility hosts a 6 MV EN Tandem electrostatic Van der Graaff accelerator with a heavy ion microbeam line. Measurements with a proton nuclear microprobe were performed at the AIFIRA facility in CENBG, Bordeaux in France. This facility is equipped with a commercially available HVEE 3.5 MeV Singletron accelerator, delivering light ions (protons, deuterons, and helium) [25, 26]. At both sites, the microbeam line with a focus of approximately 1 μm in diameter enables the collected charge to be precisely mapped.

During the experiment, the scCVD diamond membrane based microdosimeter prototype was mounted inside of a vacuum chamber. The upper strip electrode (see Figure 4) was then connected to the charge sensitive readout electronics, which included as a first stage a low noise CoolFet Amptek 250 preamplifier [27]. In general, we used positive polarity input signals as microdosimeter signal readout. The recorded data was processed into mean charge collection maps (pulse-height) or so-called hit maps, corresponding to the number of counts/interactions per pixel.

When charged particles pass through a target material (e.g., diamond microdosimeter), they lose kinetic energy. In Figure 6, the SRIM simulated energy loss (equivalent to lineal energy) [28] demonstrates the difference between 2.0 MeV protons and 16.6 MeV carbon ions passing through a diamond material.

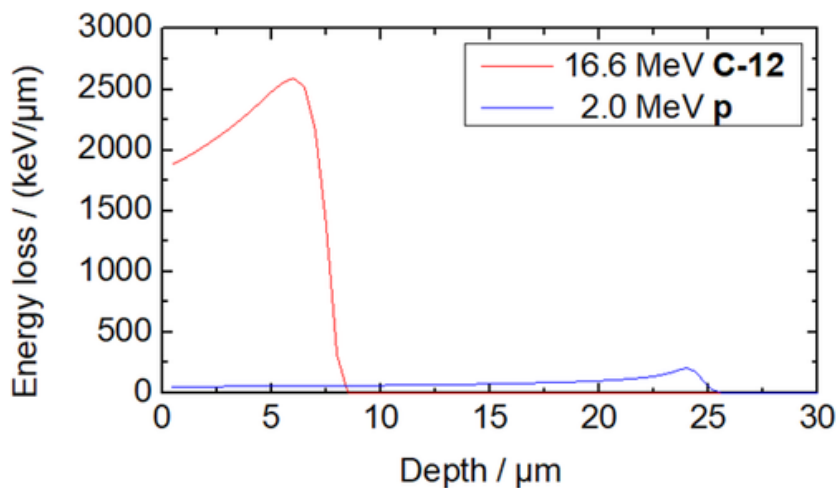


Figure 6 SRIM simulation of protons and carbon ions energy loss within diamond. Due to their lower linear energy transfer (LET) protons penetrate diamond material much deeper than carbon ions. The green dashed line marks the thickness of the diamond membrane and demonstrates that both projectiles are able to penetrate the membrane at the given energies.

The green dashed line represents the thickness of the scCVD diamond membrane based microdosimeter, thus demonstrating that both projectiles fully penetrate the membrane at the energies used in this study. By integrating the simulated energy loss between 0 and 4 μm , a rough estimation of the measured energy corresponding to a theoretical LET value of $50 \text{ keV } \mu\text{m}^{-1}$ for protons and $1863 \text{ keV } \mu\text{m}^{-1}$ for carbon ions can be made [28]. These values almost correspond to both extremities of the LET range used in hadron therapy (protons and carbon ions).

3 Results I

3.1 Preliminary Laboratory Tests

Before testing the prototype, a scCVD diamond membrane with only one large single p^+ -layer (as shown in Figure 3d) was tested in laboratory conditions with a 5.5 MeV Am-241 α -source. A classical charge sensitive electronics chain, including a low noise preamplifier, Amptek CoolFet A250 [27] was used.

In Figure 7, two pulse-height spectra of 5.5 MeV alpha particles traversing this diamond membrane of 4 μm are displayed. In black the signal detected with no applied external bias and in red with a +16 V applied bias to the device can be distinguished. The latter corresponds to an applied electric field of $3.2 \text{ V } \mu\text{m}^{-1}$, which is a field strength significantly exceeding the value of $0.3 \text{ V } \mu\text{m}^{-1}$ at which a 100%

CCE is expected for an electronic grade diamond material from Element Six [20]. Furthermore, a strong indication of a full CCE at 0 V bias can be made due to the significant similarity of both detected spectra.

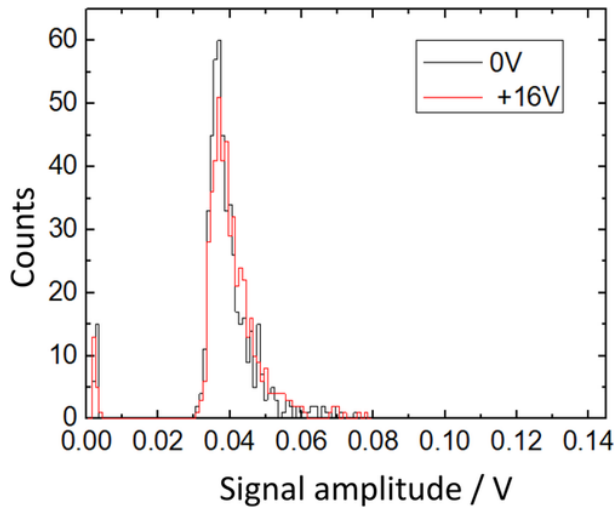


Figure 7 Pulse-height spectra detected by a scCVD diamond membrane with only one large single p^+ -layer μ SV during the exposure to a 5.5 MeV Am-241 α -source. No bias (in black) and a +16 V external bias (in red) were applied to the device. The strong similarity of both spectra suggests a 100% CCE at 0 V bias.

3.2 Response of the Diamond Microdosimeter to Ion Microbeams – Micro-Sensitive Volumes Definition

The self-biased scCVD diamond membrane based microdosimeter prototype (Figures 4 and 5) was raster scanned with 2.0 MeV protons and 16.6 MeV carbon ions microbeam in different spatial areas.

In Figure 8a a global hit map resulting from a raster scanned area with 2.0 MeV protons of the self-biased diamond membrane is shown. Here, the positive input polarity of the microdosimeter signal was used as a readout. This hit map with colour-coded pixels represents the detected ion interactions within the diamond membrane. The colours pink up to orange, represent a high number of hits per pixel, with those in black representing no detected interactions. According to our concept of the p^+ -i-m and m-i-m junction, it can be observed that only the regions of p^+ and intrinsic diamond (i) μ SVs covered with Al contacts are active and register ion hits. This result confirms our concept previously explained in section 2.1. In Figure 8b a microscopic picture of the exact same region of the device as in Figure 8a is shown. From directly comparing both images, significant changes in the size, shape and position of the micro-sensitive volumes can be excluded. Similar results were observed for the 16.6 MeV carbon ion microbeam raster scan of the same device.

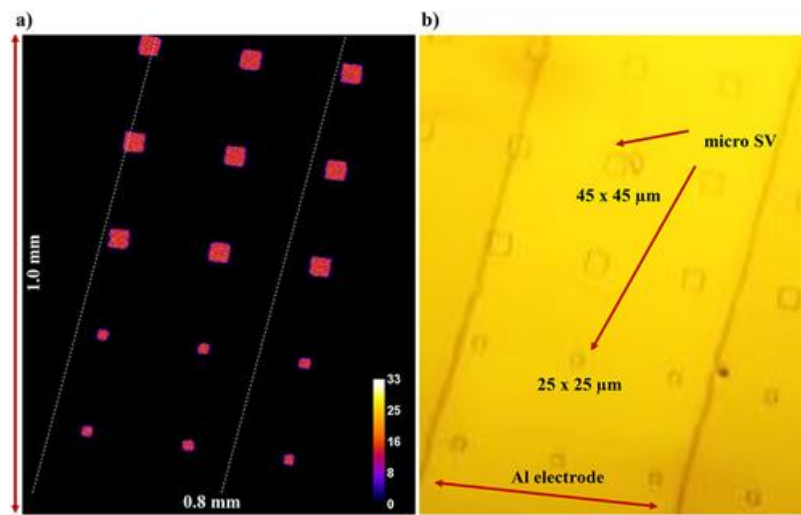


Figure 8 a) Response of diamond membrane microdosimeter to a global raster scan at 0 V bias with 2 MeV proton microbeam. b) A microscopic image of the exact same spatial region as raster scanned image.

In Figure 9, mean charge collection (pulse-height) maps from single raster scanned μ SVs and their corresponding pulse-height spectra are shown. On the left side in Figure 9a, the deposited energy distribution in a $25 \times 25 \mu\text{m}^2$ μ SV from the proton microbeam and in Figure 9b in a $45 \times 45 \mu\text{m}^2$ μ SV from the carbon ion microbeam is presented. The spectra plotted in blue and red represent the pulse-heights distribution for all events detected from the full area as shown left in the mean charge collection maps. These spectra include the area outside the μ SV as well as its edges. For both ion types, the deposited energy distribution peak is well defined, but an additional tail at lower energies appears. At first, it appears that the lower tail signal was more pronounced for proton irradiation than carbon, however, the contribution of incomplete charge collection signal to the spectra is linked to the size of the investigated μ SV. The larger the μ SV the smaller the contribution due to ratio between inside of the μ SV and the edges, which might be the origin of the lower signal. Furthermore, the green spectra in Figure 9a,b correspond to the events located only in the centre of the μ SV (indicated by the green box). These spectra do show a perfect definition of FWHM with no tail contributing to lower energies and are ideal for lineal energy measurements in clinical settings.

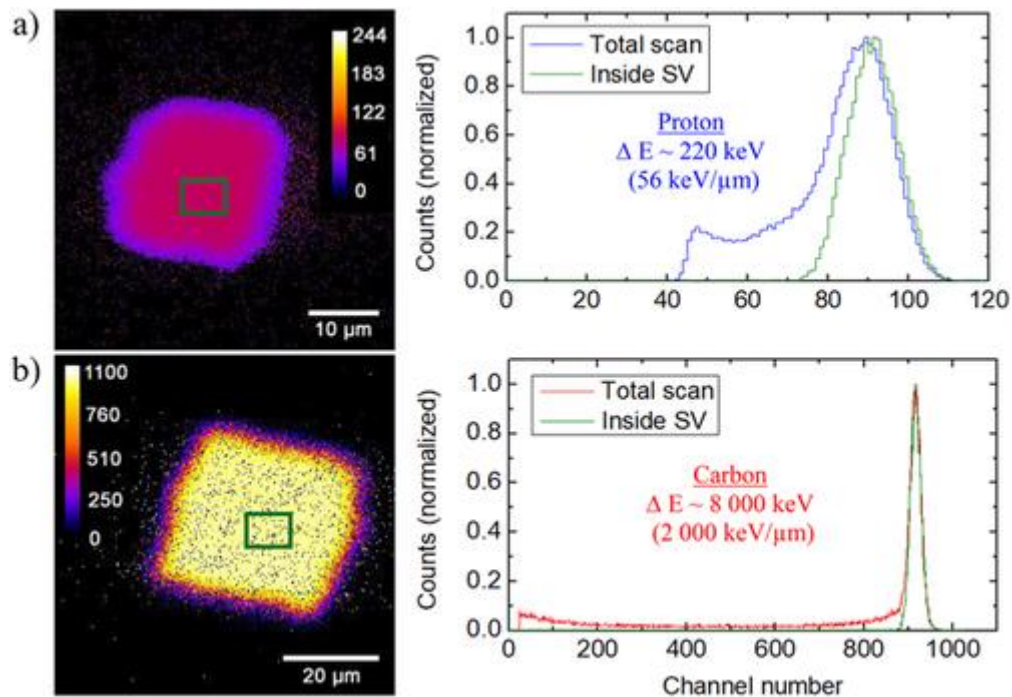


Figure 9 Response of the scCVD diamond membrane based microdosimeter to a) 2 MeV protons and b) 16.6 MeV carbon ions. (Left) Mean pulse-height maps and (Right) pulse-height spectra at 0 V bias applied to the device.

A closer analysis of the origin of the low energy tail has been made for proton irradiation. In Figure 10, different regions of the pulse-heights distribution and their corresponding hit maps are shown.

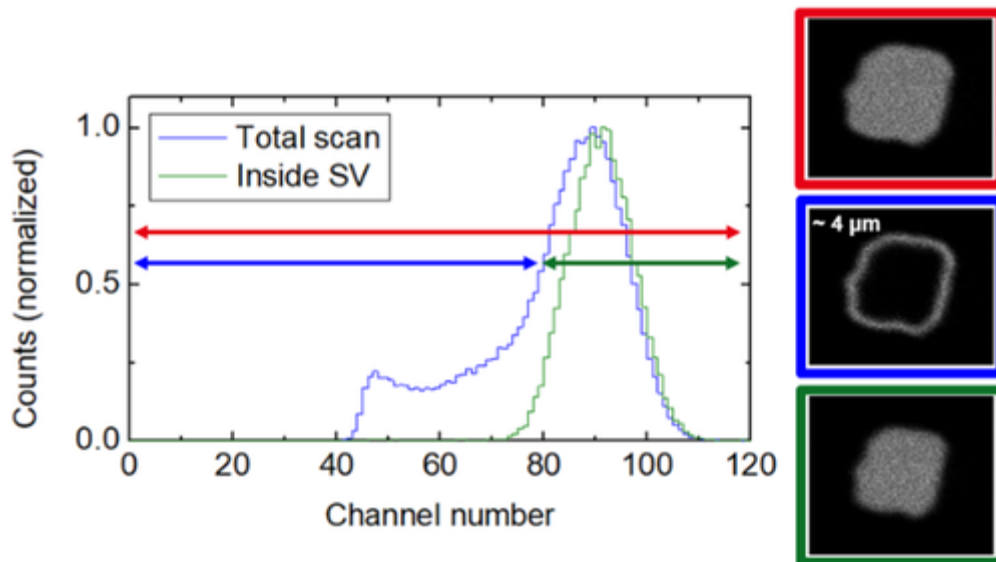


Figure 10 Analysis of the pulse-height spectra and the tail at lower energies. Displayed hit maps clearly identify the region of low energy contribution, which is linked to a reduced CCE at the edges of the μ SV. The imperfect defined edges produce an approximately $4 \mu\text{m}$ large region of reduced CCE signal around the μ SV.

It can be clearly seen that the lower energy signals are related to the incomplete CCE close to the edges of the μ SV.

Furthermore, in Figure 11 a hit map is shown which was obtained at 0 V, accepting only negative polarity signals from the microdosimeter and the corresponding pulse-height spectra. In the large m-i-m region (outside of the μ SVs) a weak residual signal can be observed. The generated signal is inverted in polarity and about 20 times weaker than the positive polarity signals from μ SVs. This can be better translated to much narrower depletion zones, thus charge displacement achieved. This effect is most likely to occur as a result of imperfect ohmic contact between the metal and diamond material, in which surface-pinning states are then introduced. This could also be due to the surfaces of the diamond sample not being perfectly cleaned prior to Al coating, as slight irregularities in the shape regions would not significantly affect the signal. Another point is that slightly higher than average signals are induced at the electrodes borders/interfaces and small-localized defects (circled red) appear. These defects are most probably structural-like dislocations or bundles of dislocations.

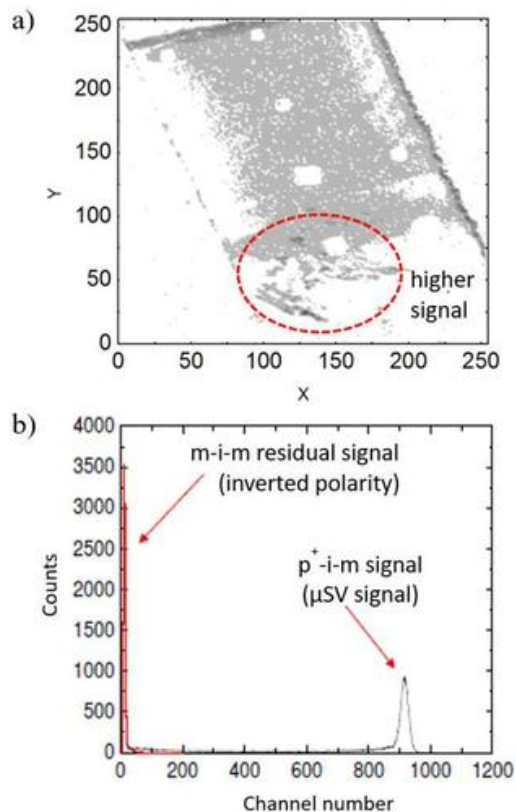


Figure 11 a) A hit map image with marked regions of higher-than-average signal and b) pulse-height spectrum of the scCVD diamond membrane based microdosimeter for inverted polarity of generated signal acquired at 0 V.

It is also more likely that at these sites a non-isotropic strain is introduced into the diamond bulk which can result in non-isotropic diffusion and thus signal generation. These effects can also result in partial drift and thus residual signal formation with a reduced CCE. However, as these have an opposite polarity with respect to the main signal, they are easy to differentiate from such, and thus do not contribute negatively to the signal formation under normal operating conditions of the microdosimeter.

Possible changes in the design and production of the diamond-based microdosimeter could improve the shape of the pulse-height spectra. This could be obtained for example by introducing radiation damage (ion implantation) to the areas outside of μ SVs. Also, aspects of ohmic-contact formation must be explored in more detail.

Finally, compared with the responses of silicon-based microdosimeters [9] to ion microbeams, the results from the scCVD diamond membrane based microdosimeter show already very good characteristics and a good agreement with the theoretical values, confirming the microdosimeter's ability to measure microdosimetric quantities in single ion beams.

3.3 Charge Collection Efficiency

Figures 12 and 13 show the charge collection characteristics of a single μ SV (p^+ -i-m) and the region outside of it (m-i-m), while applying different bias voltage ranging from -5 to $+5$ V. The red curve corresponds to the values measured under irradiation of the proton microbeam and blue under irradiation of the carbon ion microbeam. Pulse-height is normalized to maximum measured value at relatively high electric field which should represent 100% CCE in electronic grade scCVD material. The following important parameters can be extracted from these graphs.

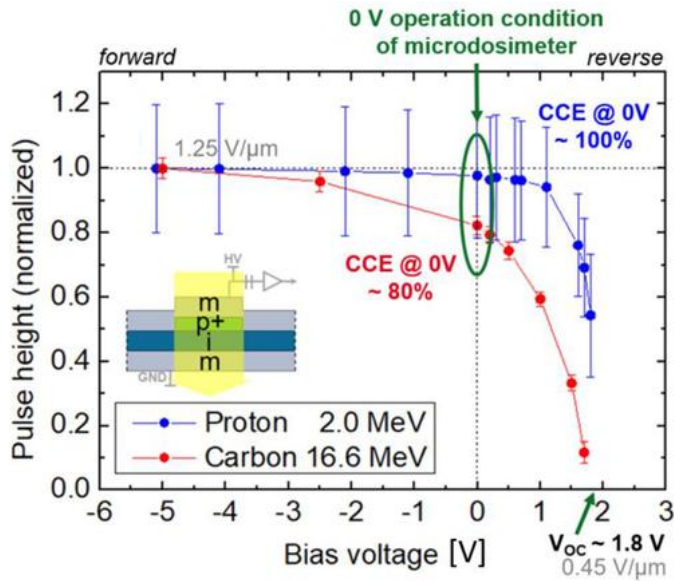


Figure 12 Charge collection characteristics vs. microdosimeter bias voltage inside of a micro-sensitive volume. At 1.8 V a built-in potential and thus electric field of $0.45 \text{ V } \mu\text{m}^{-1}$ for our device, can be measured. For the operation condition at 0 V a CCE of almost 100% for protons only 80% for carbons was reached.

In Figure 12, the intersection of the x -axis at -1.8 V corresponds to the flat band conditions where the internal electric field is compensated by the externally applied bias and equals zero and was previously measured to identical value for other devices [18]. This shows the built-in potential within the μSVs due to the p^+i - m junction formation between the intrinsic diamond membrane and the boron-doped diamond electrode, corresponding to an electric field of $0.45 \text{ V } \mu\text{m}^{-1}$ for this device. For the operational condition at 0 V for protons, almost 100% CCE was observed. However, for carbon ions, which have a higher linear energy (LET) than protons, pulse-height defects appeared and therefore a CCE of only 80% was reached. At this point the electric field of $0.45 \text{ V } \mu\text{m}^{-1}$ is not enough to efficiently separate e-h pairs created from dense ionization, and thus some recombine. This recombination effect could be reduced if a thinner membrane (e.g., $1.4 \mu\text{m}$) is used, as 100% CCE is reached at around $1.25 \text{ V } \mu\text{m}^{-1}$, even for carbon ions.

In Figure 13, as expected for the m - i - m junction at 0 V, no charge collection for both particle types was observed. Additionally, for both polarities quick saturation of collected charge was observed, as was expected for electronic grade material. A small shift in the saturated levels for positive and negative biases can be explained by ADC offset, which was not corrected in these measurements.

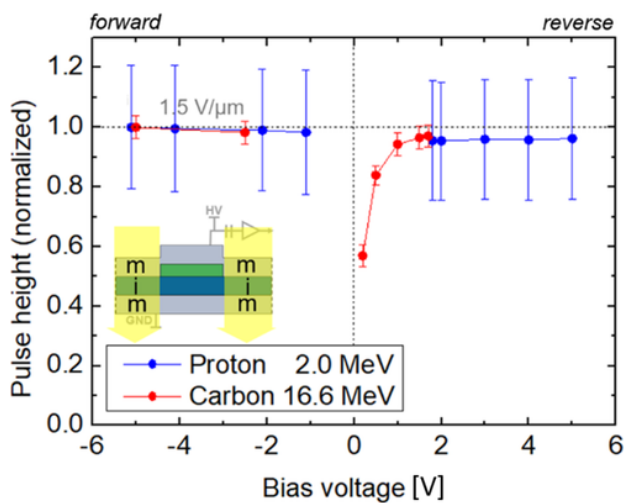


Figure 13 Charge collection characteristics vs. microdosimeter bias voltage outside of a micro-sensitive volume. No significant charge collection for the m - i - m junction at 0 V was detected.

3.4 Insight into Radiation Hardness

Compared to classical radiotherapy where gammas or electrons are used, particle therapy dosimetry or microdosimetry devices must deal with much higher radiation damage risk. Charge particles interacting with semiconductor material will create primary defects like vacancies and interstitials which will strongly contribute to life time reduction of charge carriers. This can result in a reduced CCE, thus altering the performance of the scCVD diamond membrane based microdosimeter. Preliminary radiation hardness tests were performed to determine the device's suitability for medical applications. A single μSV and surrounding regions were irradiated locally by means of proton and carbon microbeam. The results are presented in Figure 14a,b.

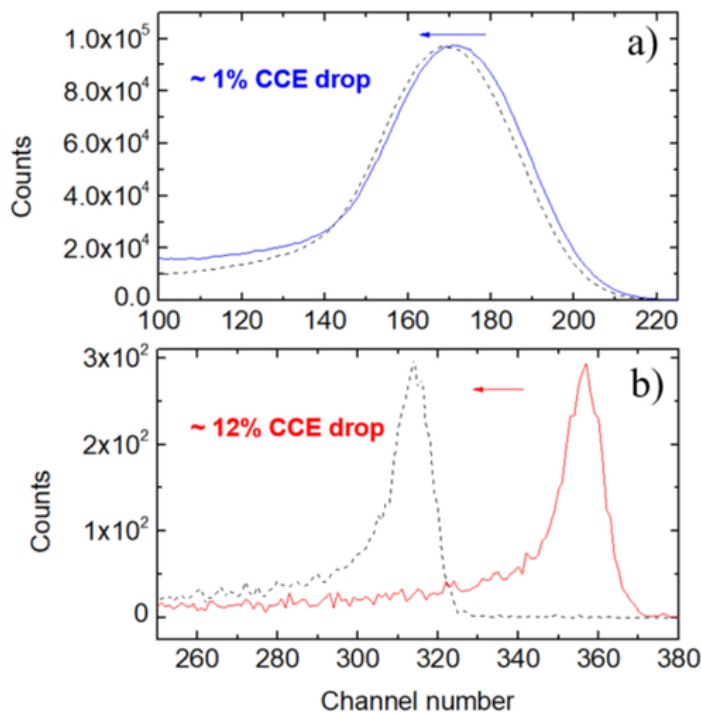


Figure 14 Pulse-height spectra from the scCVD diamond membrane based microdosimeter before (solid line) and after (dashed line) exposure to a high a) proton and b) carbon ion fluence.

Figure 14a shows the pulse-height spectra of a single μSV s irradiated with up to 2.5×10^{13} ions per cm^2 . This high fluence of protons caused only a 1% drop of the CCE of the device. For heavier carbon ions, shown in Figure 14b, a drop of 12% was observed after 0.64×10^{12} carbon ions per cm^2 . Although, the fluence in the particle therapy with carbon ions is much lower than for protons. This means that these presented results are very good even for carbon ions.

It is also important to note that any changes in the spectrum shape, peak FWHM or μSV geometry were insignificant. With these results, over 500 treatments for both particle types would be possible before a CCE drop of 1%.

4 Results II

4.1 Preliminary Measurements in Clinical Proton Beam

Preliminary tests of a scCVD diamond membrane based microdosimeter in mixed radiation field were conducted at the Institute Curie – Proton Therapy Centre in Orsay. The therapy centre hosts the C235 cyclotron which delivers proton beams with energies of up to 235 MeV in both scattered and pencil beam scanning modes [29].

For the purpose of this study, a 100 MeV clinical proton beam in scattered scanning mode was used. The readout of previously tested μSV s was performed with a low noise CoolFet Amptek 250 preamplifier, and classical charge sensitive chain including Amptek MCA-8000 Multichannel analyzer [27]. As shown in Figure 15, the diamond membrane device was placed on the movable patient

treatment table and centred in front of the proton beam with help of Gafchromic films. The so-called plastic water plates were used to simulate different depth in the water phantom or patient body. In Figure 16, dose-weighted-microscopic distributions were obtained by applying algorithms [30] to the measured pulse-height spectra from the scCVD diamond membrane based microdosimeter at three different experimental points as shown in Figure 16 (inset): the entrance at 0 mm (1), and the Bragg peak regions at 68 mm (2) and 78 mm (3). The spectrum (in non-calibrated units) represents the spread of the lineal energy over two decades.

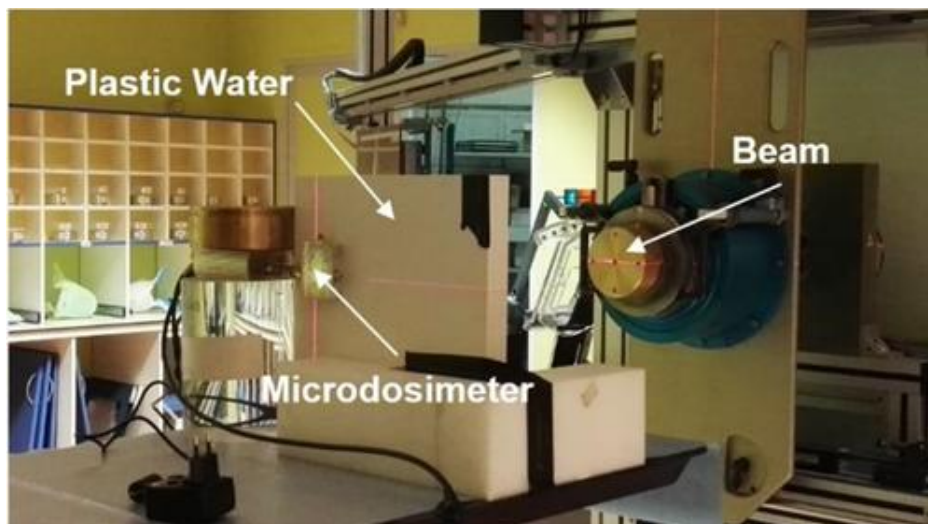


Figure 15 A picture of the experimental setup at the Institute Curie – Proton Therapy Centre in Orsay with a 100 MeV clinical proton beam.

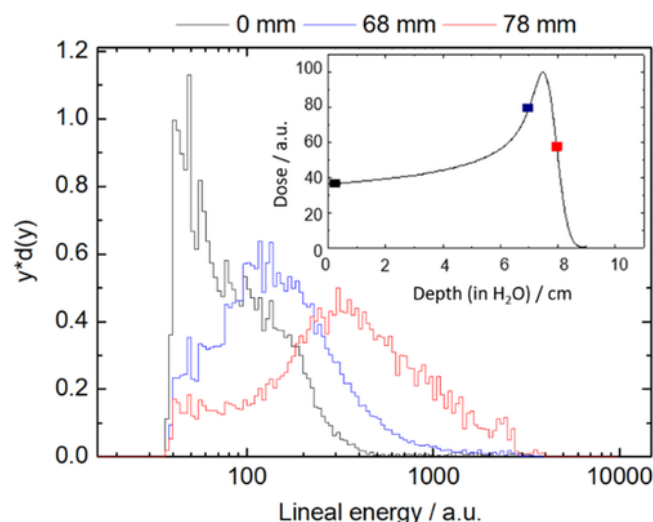


Figure 16 Microscopic spectra obtained using the scCVD diamond membrane based microdosimeter at three different experimental points. Inset: Simulated Bragg peak of a 100 MeV therapeutic beam in a water phantom with experimental points taken at 0, 68, and 78 mm depths.

Although not calibrated with the energy and therefore not directly comparable to related microdosimeters responses, a general trend can be observed in which there is an increase in pulse-height (lineal energy) at higher energies (distal part) for the Bragg peak. However, this similar behavior of the scCVD diamond membrane based microdosimeters can be also observed for known measurements obtained from TEPC [11] and silicon dosimeters [9, 12, 13, 31], which demonstrates the microdosimeter's ability to measure microdosimetric quantities in clinical ion beams.

5 Summary and Outlook

Initial prototypes of scCVD diamond membrane based microdosimeters have been characterised with 2.0 MeV proton and 16.6 MeV carbon ion microbeams. Furthermore, preliminary measurements in mixed radiation fields at the Institute Curie – Proton Therapy Centre, Orsay with 100 MeV clinical proton beam have been conducted.

The present results from the prototypes demonstrate that scCVD diamond membrane based microdosimeters are relatively easy to fabricate and provide high spatial resolution measurements. When operated at 0 V, a CCE of almost 100% for protons and 80% for carbons was reached with good spatial definition of μSV .

Furthermore, the radiation hardness tests have demonstrated the device's suitability for medical applications. Possible optimization of the μSVs signal could be achieved by introducing radiation damage due to ion implantation.

Finally, preliminary tests in clinical environments with therapeutic proton beams have shown typically expected lineal energy characteristics of a 100 MeV therapeutic proton beam. Additionally, very good characteristics were observed compared with other micro-detectors like TEPC and silicon-based microdosimeters.

Acknowledgements

This research has been performed within the framework of the DIAMiDOS (Diamond membrane microdosimeter) project founded by the French Alternative Energies and Atomic Energy Commission (CEA). The authors would like to acknowledge DiamFab.eu for growing excellent quality homoepitaxial p^+ diamond films. Furthermore, the authors would like to thank all collaboration partners and especially the IBIC microbeam teams in Ruđer Bošković Institute in Zagreb, Croatia and AIFIRA facility of CENBG in Bordeaux, France. This project has received funding from the European Union's Horizon 2020 Research and Innovation programme under Grant Agreement no. 654168.

Conflict of Interest

The authors declare no conflict of interest.

References

- [1] World health statistics (WHO) 2017. Licence: CC BY-NC-SA 3.0 IGO.
- [2] G. Kraft, *Prog. Part. Nucl. Phys.* 2000, 45, 473.
- [3] J. S. Loeffler, M. Durante, *Nat. Rev. Clin. Oncol.* 2013, 10, 411.
- [4] M. Scholz, A. M. Kellerer, W. Kraft-Weyrather, G. Kraft, *Radiat. Environ. Biophys.* 1997, 36, 59.
- [5] R. B. Hawkins, *Med. Phys.* 1998, 25, 1157.
- [6] H. Paganetti, *Phys. Med. Biol.* 2014, 59, 419.
- [7] C. Grassberger, A. Trofimov, A. Lomax, H. Paganetti, *Int. J. Radiat. Oncol., Biol., Phys.* 2011, 80, 1559.
- [8] International Commission on Radiation Units and Measurements (ICRU) Report: 16, Linear Energy Transfer ICRU, Maryland, 1970.
- [9] A. B. Rosenfeld, *Nucl. Instrum. Methods Phys. Res., Sect. A* 2016, 809, 156.
- [10] H. H. Rossi, W. Rosenzweig, *Radiology* 1955, 64, 404.

- [11] M. Farahmand, A. J. J. Bosa, J. Huizengaa, L. De Nardob, C. W. E. van Eijka, *Nucl. Instrum. Methods Phys. Res., Sect. A* 2003, 509, 262.
- [12] L. T. Tran, L. Chartier, D. Bolst, A. Pogosso, S. Guatelli, M. M. L. F. Petasecca, Lerch, D. A. Prokopovich, M. I. Reinhard, B. Clasié, N. Depauw, H. Kooy, J. B. Flanz, A. McNamara, H. Paganetti, C. Beltran, K. Furutani, V. L. Perevertaylo, M. Jackson, A. B. Rosenfeld, *Med. Phys.* 2017, 44, 6085.
- [13] L. T. Tran, L. Chartier, D. A. Prokopovich, D. Bolst, M. Povoli, A. Summanwar, A. Kok, A. Pogosso, M. Petasecca, S. Guatelli, M. I. Reinhard, M. Lerch, M. Nancarrow, N. Matsufuji, M. Jackson, A. B. Rosenfeld, *IEEE Trans. Nucl. Sci.* 2018, 65, 467.
- [14] C. Verona, G. Magrinb, P. Solevic, M. Bandorfb, M. Marinellia, M. Stockb, G. Verona Rinatia, *Radiat. Meas* 2018, 110, 25.
- [15] J. A. Davis, S. Guatelli, M. Petasecca, M. L. F. Lerch, M. I. Reinhard, M. Zaider, J. Ziegler, A. B. Rosenfeld, *IEEE Trans. Nucl. Sci.* 2014, 61, 1544.
- [16] C. Moignier, D. Tromson, F. Marsolat, L. De Marzi, M. Pomorski, M. Agelou, J. Garcia Hernandez, D. Lazaro, A. Mazal, *Med. Phys.* 2016, 43, 3502.
- [17] C. Moignier, D. Tromson, L. De Marzi, F. Marsolat, J. Carlos, G. Hernándezl, M. Agelou, M. Pomorski, R. Woo, J. M Bourbotte, F. Moignau, D. Lazarol, A. Mazal, *Phys. Med. Biol.* 2017, 62, 5417.
- [18] C. Delfaure, M. Pomorski, J. De Sanoit, P. Bergonzo, S. Saada, *Appl. Phys. Lett.* 2016, 108, 2521.
- [19] C. Cazzaniga, M. Rebai, J. Garcia Lopez, M. C. Jimenez-Ramos, M. Girolami, D. M. Trucchi, A. Bellucci, C. D. Frost, M. Garcia-Munoz, M. Nocente, M. Tardocchi, G. Gorini, *Nucl. Instrum. Methods Phys. Res., Sect. B* 2017, 405, 1.
- [20] <https://amptek.com>
- [21] <https://www.almax-easylab.com>
- [22] M.-A. Pinault-Thaurya, F. Jomarda, C. Mer-Calfati, N. Tranchant, M. Pomorski, P. Bergonzo, J.-C. Arnault, *Appl. Surf. Sci.* 2017, 410, 464.
- [23] M. Pomorski, B. Caylar, P. Bergonzo, *Appl. Phys. Lett.* 2013, 103, 112.
- [24] M. Jaksic, I. Bogdanovic Radovic, M. Bogovac, V. Desnica, S. Fazinic, M. Karlusic, Z. Medunic, H. Muto, Z. Pastuovic, Z. Siketic, N. Skukan, T. Tadic, *Nucl. Instrum. Methods Phys. Res., Sect. B* 2007, 260, 114.
- [25] G. Devès, L. Daudin, A. Bessy, F. Buga, J. Ghanty, A. Naar, V. Sommar, C. Michelet, H. Sez nec, P. Barberet, *Nucl. Instrum. Methods Phys. Res., Sect. B.* 2015, 348, 62.
- [26] S. Sorieul, P. Alfaut, L. Daudin, L. Serani, P. Moretto, *Nucl. Instrum. Methods Phys. Res., Sect. B* 2014, 332, 68.
- [27] <https://amptek.com>
- [28] J. F. Ziegler, *SRIM*. 2013.

[29] A. Patriarca, S. Meyroneinc, *Triumpf: Proc. of Cyclotrons (WEPSH010)*. 2013, 403. (ISBN: 978-3-95450-128-1)

[30] S. Najm Al-Bayati, *Master of Applied Science*, University of Ontario, Institute of Technology 2012, 97. (<https://ir.library.dc-uoit.ca/handle/10155/294>)

[31] S. E. Anderson, K. M. Furutani, L. T. Tran, L. Chartier, M. Petasecca, M. Lerch, D. A. Prokopovich, M. Reinhard, V. L. Perevertaylo, A. B. Rosenfeld, M. G. Herman, C. Beltran, *Med. Phys.* 2017, 44, 6029.